Magnetization oscillations induced by a spin-polarized current in a point-contact geometry: Mode hopping and nonlinear damping effects

D. V. Berkov and N. L. Gorn
Innovent Technology Development e.V., Pruessingstrasse 27B, D-07745 Jena, Germany
(Received 9 May 2007; published 11 October 2007)

In this paper, we study magnetization excitations induced in a thin extended film by a spin-polarized dc current injected through a point contact in the current-perpendicular-to-plane geometry. Using full-scale micromagnetic simulations, we demonstrate that in addition to the oscillations of the *propagating* wave type, there exist also *two localized* oscillation modes. The first localized mode has a relatively homogeneous magnetization structure of its core and corresponds to the so-called "bullet" predicted analytically by Slavin and Tiberkevich [Phys. Rev. Lett. **95**, 237201 (2005)]. Magnetization pattern of the second localized mode core is highly inhomogeneous, leading to a much lower power of magnetoresistance oscillations caused by this mode. We have also studied the influence of a *nonlinear damping* for this system and have found the following main qualitative effects: (i) the appearance of frequency jumps within the existence region of the propagating wave mode and (ii) the narrowing of the current region where the bullet mode exists, until this mode completely disappears for a sufficiently strong nonlinear damping.

DOI: 10.1103/PhysRevB.76.144414 PACS number(s): 75.40.Gb, 75.40.Mg, 85.75.−d, 75.75.+a

I. INTRODUCTION

Since Slonczewski[1] and Berger[2] predicted that a spin-polarized current flowing through a thin magnetic film can induce magnetization excitations (up to a complete magnetization switching) and first experimental confirmations of this effect[3] were obtained, the spin-torque induced magnetization dynamics belongs to the most intensively studied topics of the solid state magnetism.[4]

Most experiments in this area have been performed in the so-called columnar geometry, i.e., for a system where an electric current flows through a "sandwich" structure consisting of two or more thin ferromagnetic layers with lateral sizes in the region ~50–200 nm separated by nonmagnetic spacers. Here, a substantial degree of understanding has been achieved due to high-quality experimental studies,[5] detailed theoretical analysis,[6] and extensive numerical simulations[7] (citations given above are by no means exhaustive).

In contrast to this situation, the interpretation of experimental results for the magnetization dynamics in the so-called point-contact geometry remains controversial.[8–13] On the one hand, this is due to a much more complicated nature of point-contact systems compared to nanopillars. In particular, the macrospin approximation, being of some help for a small nanoelement, is absolutely invalid in the point-contact setup due to a strong exchange interaction between the oscillating area under the contact with the rest of a thin film. On the other hand, the accumulated body of experimental results is much smaller than for the columnar geometry, so that a quite limited amount of data is available for a comparison with analytical theories and numerical simulations.

Even the type of spin-wave excitations induced in the point-contact experiments remains a subject of an intensive discussion. In particular, experimental threshold of the magnetization oscillations onset for the *in-plane* external field is significantly lower than the value predicted by Slonczewski for the linear spin-wave mode,[8] as it was pointed out in Ref. 10 (when the external field is applied *normally* to the film plane and is strong enough to ensure the out-of-plane magnetization of a film, the result of Slonczewski shows a good agreement with experimental data). Another important point is that the oscillation frequency observed, e.g., in the pioneering experiment of Rippard *et al.*[9] (for an in-plane applied field), is smaller than the homogeneous FMR frequency for the thin layer with magnetic parameters reported in Ref. 9, so that an *extended* spin wave with such a frequency could not exist. Basing on these indications, Slavin and Tiberkevich suggested that the spin-wave mode excited under conditions used in Ref. 9 is a nonlinear localized mode[10,11] for which the excitation threshold and oscillation frequency turned out to be significantly smaller than for the linear propagating wave mode.

The analytical theory of Slavin and Tiberkevich employs several approximations, unavoidable in such situations (see Refs. 10 and 11 for details) and as such should be verified by rigorous numerical simulations. However, as we have already pointed out in Ref. 13, numerical simulations of magnetization dynamics in the point-contact setup encounter several serious methodical difficulties, which partly explains why corresponding studies are extremely rare. In Ref. 13, we have explained how these difficulties can be overcome and made an attempt to reproduce experimental results from Ref. 9 by simulating the complete trilayer system $Ni_{80}Fe_{20}$(5 nm)/Co(5 nm)/$Co_{90}Fe_{10}$(20 nm) studied in Ref. 9 including also the Oersted field effect. We have found that the magnetization dynamics in such a system is extremely complicated. Moreover, we have observed qualitative disagreement between our simulations and experimental data. For these reasons and taking into account also that (i) magnetic parameters and especially the polycrystalline structure of the "fixed" $Co_{90}Fe_{10}$ layer are not known well enough and (ii) reliable evaluation of the Oersted field effect without the exact knowledge of the current distribution is not possible, we decided to perform systematic studies of the simplest possible point-contact setup where the onset of the magnetization dynamics due to the spin torque can be expected: a

single magnetic layer subject to a spin-polarized current within the point-contact area (with the Oersted field neglected). As we shall demonstrate below (Sec. III A), despite these simplifications, results of our study reveal many important aspects of the spin-wave dynamics in such systems (including the existence of several excitation modes) and allow a meaningful comparison both with analytical theories[10,11] and experimental data.[9]

In addition, we have studied the effect of a nonlinear damping (damping depending on the magnetization change rate, as suggested in Ref. 14) because for the large-angle spin-torque-driven magnetization oscillations, such effects are expected to be especially strong. Corresponding results are presented in Sec. III B.

II. SIMULATED SYSTEM AND SIMULATION METHODOLOGY

As explained above, to make the system under study as simple as possible, but still retaining the whole nontrivial physics, we have simulated the dynamics of a system consisting of a "free" layer only with magnetic parameters corresponding to $Ni_{80}Fe_{20}$ (Permalloy) layer in the experiments described in Ref. 9: saturation magnetization $M_S=640$ G, exchange stiffness constant $A=1\times10^{-6}$ erg/cm, negligible magnetocrystalline anisotropy, and layer thickness $h=5$ nm. For all results presented below, the external field $H_{\text{ext}}=1000$ Oe was applied in the film plane. The x axis of our coordinate system is directed along the external field; the z axis is the second Cartesian axis *in the film plane*, so that the y axis is *perpendicular* to the film. Simulated area with the in-plane size of 900×900 nm^2 was discretized into $N_x\times N_z\times N_y=360\times360\times1$ cells, so that the cell size was $2.5\times2.5\times5$ nm^3; periodic boundary conditions (PBCs) were used. Diameter of the current flooded area $D=40$ nm also corresponds to the nominal point contact diameter reported by Rippard *et al.*[9] It is important to note that due to such a small diameter discretization, the cell size larger than used by us (see above) led to inadequate discretization of this area and caused substantial artifacts by simulating the magnetization dynamics—especially when the second localized mode with a fine spatial structure was excited.

The Oersted field of the spin-polarized current was neglected for three reasons. First, the presence of this field lead to a much more complicated magnetization dynamics and we intended to study the minimal nontrivial model to emphasize the effects of the mode localization and nonlinear damping as clear as possible. Second, the proportionality coefficient between the spin-torque amplitude used in simulations and the current strength (which determines the magnitude of the external field) is not known exactly. Third, the electric current distribution in the experimental setup is also known to be relatively poor, adding another uncertainty to the Oersted field evaluation.

To suppress artificial interference between the "original" spin wave emitted from the point-contact area (placed in the center of the simulated square) and waves coming from PBC replica of the initial system, we have employed our method based on the spatially dependent damping coefficient (see Ref. 13 for details). In addition, we have smoothed the spatial current distribution also in the same manner as in Ref. 13 to avoid artificial generation of the magnetization pattern with the wavelength twice the cell size inside the point-contact area (which appears otherwise due to the abrupt jump of the current density at the border of the area below the point contact).

Magnetization dynamics excited by a spin-polarized current was simulated using basically the same software package as in Ref. 13 (which is the extension of our commercially available MICROMAGUS package—see Ref. 15 for implementation details). Thermal fluctuations were neglected ($T=0$). Spin torque acting on the magnetization $\mathbf{M}$ was included into the Landau-Lifshitz-Gilbert (LLG) equation of motion in a meanwhile standard way via the additional term $\Gamma_{\text{st}}=a_J[\mathbf{M}\times(\mathbf{M}\times\mathbf{p})]$, where $\mathbf{p}$ denotes the spin polarization direction of electrons in the dc current through the device and a_J is proportional to the current strength I. In our simulations, $\mathbf{p}$ was chosen to be *opposite* to the applied field direction H_{ext} because in real point-contact experiments, the magnetization dynamics is supposed to be driven by spin-polarized electrons *reflected* from the fixed magnetic layer (of a FM/NM/FM trilayer system) toward the "free" one. The package was extended further in order to take into account nonlinear (magnetization rate dependent) damping, as suggested in Ref. 14; details of this implementation will be presented elsewhere.

III. SIMULATION RESULTS AND DISCUSSION

A. Magnetization dynamics for the linear Gilbert damping

In this section, we present the main features of the magnetization dynamics for the standard linear Gilbert damping $\Gamma_{\text{dis}}=(\lambda/M_S)\cdot[\mathbf{M}\times(d\mathbf{M}/dt)]$, where the dissipation parameter λ is constant; in simulations performed here, $\lambda=0.02$. Dependence of the magnetization oscillation frequency f on the spin-torque magnitude a_J is shown in Fig. 1(a); typical snapshots of magnetization configurations during these oscillations for various oscillation modes (see below) are shown in the same figure as grayscale maps of the $m_z(\mathbf{r})$ projection (in-plane projection perpendicular to the applied field direction).

Already for the *linear* damping, the system demonstrates a fairly rich magnetization dynamics. Oscillations start at the threshold value $a_{J,\text{th}}\approx3.55$ (±0.02) with the extended wave mode at the frequency $f\approx14.3$ GHz. This frequency is much higher than the homogeneous FMR frequency for this system ($f_{\text{FMR}}\approx8.42$ GHz) because already at the threshold, the wave with a *large* wave vector $k\sim1/R_c$ is excited due to the small radius R_c of the point contact. When the current strength (a_J value) is increased, the oscillation amplitude rapidly grows [see Fig. 1(b)], leading to the nonlinear downward frequency shift, as explained theoretically[10,11,20] and observed experimentally in several papers (see, e.g., papers of Kiselev *et al.* and Krivorotov *et al.* from Ref. 5).

When a_J exceeds the first critical value $a_{\text{cr}}^{(1)}\approx4.45$, the first frequency jump occurs: transition from the extended wave mode (W) to the localized mode of the first type (L_1)

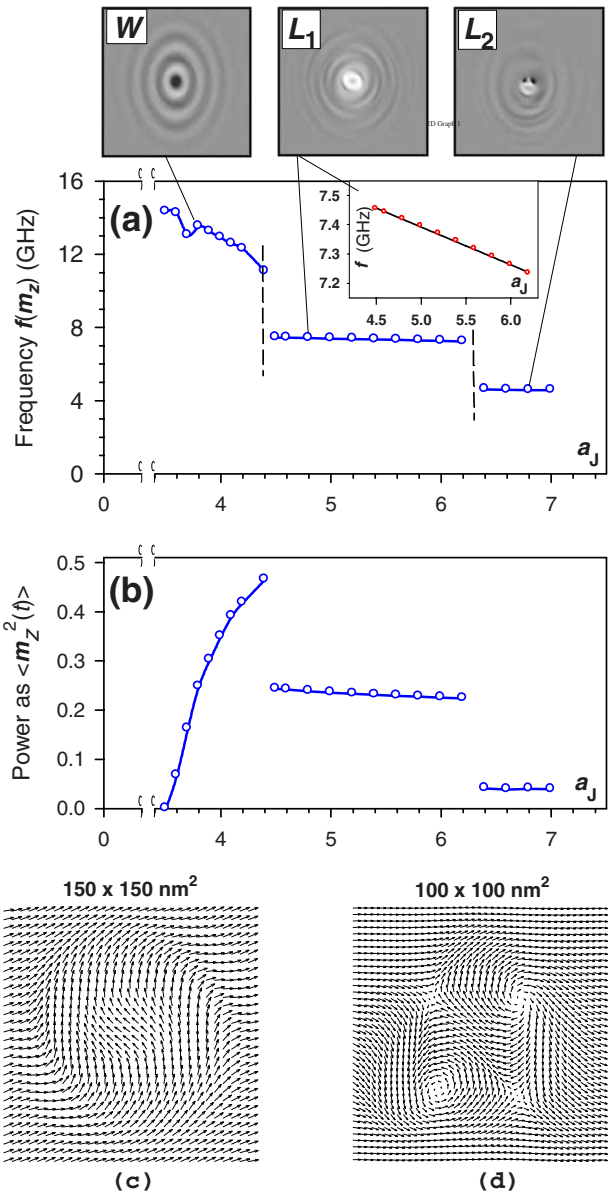

FIG. 1. (Color online) Dependencies of the (a) frequency f and (b) oscillation power P on the spin-torque magnitude a_J for the linear damping case. Frequency and power jumps accompanying the transitions from the extended wave mode W to the *localized* mode L_1 and from L_1 to the second type of the localized mode L_2 are clearly seen. Snapshots of the $m_z(\mathbf{r})$ projection (in-plane projection perpendicular to the applied field direction) for all three mode types are shown at the upper panel as grayscale maps. The inset on panel (a) demonstrates the perfectly linear frequency dependence on the current strength for the L_1 mode. Panels (c) and (d) display the in-plane magnetization projections of the localized mode cores: (c) L_1 mode (every second moment is shown) and (d) L_2 mode.

takes place. (First observations of this mode in the point-contact geometry was reported by us in Refs. 12 and 16.) The oscillation frequency drops below the f_{FMR} value—which is an immanent feature of a localized oscillation mode—and decreases linearly and very slowly from $f(a_J=4.5)\approx 7.45$ GHz to $f(a_J=6.3)\approx 7.23$ GHz [see inset in Fig. 1(a)]. A snapshot of the magnetization configuration of this

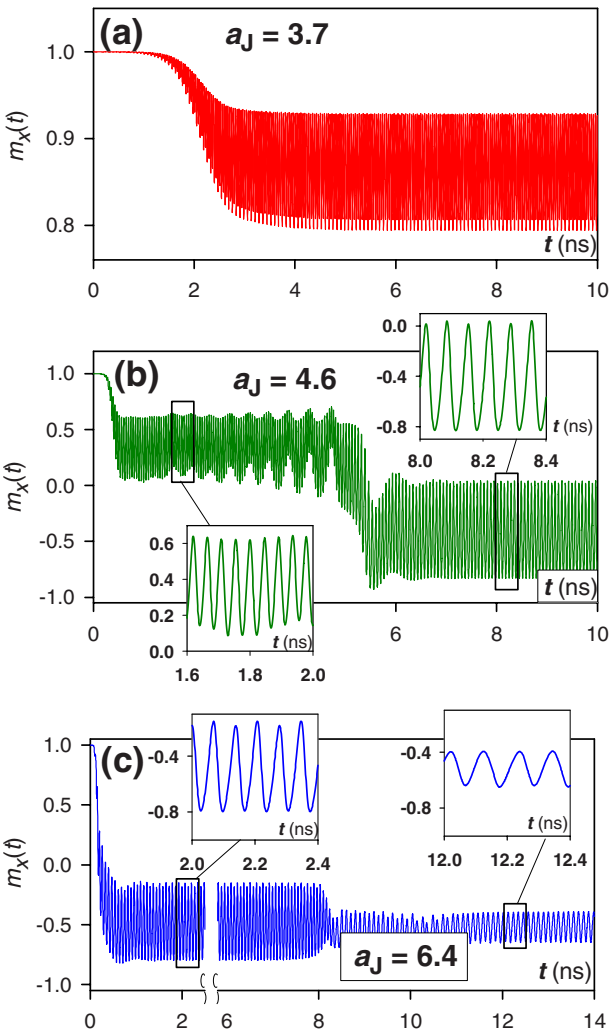

FIG. 2. (Color online) Time dependencies of the x-magnetization component (along the external field) averaged across the point-contact area for three different values of a_J: (a) magnetization oscillations for the stable extended wave mode W for $a_J=3.7$, (b) the dynamical switching process leading to the formation of the localized mode L_1, and (c) development of the second type of the localized mode L_2 from the L_1 mode. Insets demonstrate abrupt frequency jumps by the transitions between modes.

mode core is presented as the arrow plot in Fig. 1(c).

The dynamics of the transition from the W mode to the L_1 mode for $a_J > a_{\mathrm{cr}}^{(1)}$ is shown in Fig. 2(b). Here, the time dependencies of the magnetization projection $m_x(t)$ (along the external field) averaged over the point-contact area are plotted. It can be seen that after the spin current is switched on, for a_J values slightly larger than $a_{\mathrm{cr}}^{(1)}$, the extended wave mode W is excited first [left inset on Fig. 2(b)]. Then, the amplitude of magnetization oscillations increases, until the magnetization *switching* takes place, so that the magnetization begins to oscillate around the direction opposite to the applied field. The frequency jump occurring in this switching can be seen very clearly from the comparison of the two insets on Fig. 2(b).

At the second critical value $a_{\mathrm{cr}}^{(2)}\approx 6.3$, the next frequency jump accompanying the transition to the second type (L_2) of

the localized mode occurs. Typical dynamics of this transitions is shown in Fig. 2(c). The most interesting feature of this dynamics is that the formation of the second localized mode L_2 from the initial equilibrium magnetization state takes place via the intermediate formation of the first localized mode L_1. For the current values not much higher than $a_{cr}^{(2)}$, the first localized mode can still exist for times much larger than its oscillation period. We shall return to the discussion of this metastability below.

For this second spatially localized mode L_2, we show a snapshot of the spatial magnetization distribution for the whole simulated area as the grayscale map of $m_z(\mathbf{r})$ in Fig. 1(a) and as the magnetization arrow plot of the mode core in Fig. 1(d). This mode was found by us previously in the double-layer system,[13] where it was the only type of the stable localized mode. It was shown that the core magnetization structure of this mode consists of two vortex-antivortex pairs [see Fig. 1(d)]. The frequency of the L_2 mode $f \approx 4.6$ GHz remains nearly constant when the current strength is increased further. We are not aware of any analytical predictions concerning this kind of a localized mode.

It is highly instructive to analyze the dynamical transition between different mode types from the "energetical" point of view. Corresponding time dependencies of the system energy for the transition $W \rightarrow L_1$ from the extended wave mode to the first localized mode are shown in Fig. 3. Here, we display time dependencies of the energy *differences* $\Delta E = E(t) - E_0$ between the energy values $E(t)$ and the energy in the initial state E_0. We plot these differences for the total system energy E_{tot} and the standard micromagnetic contributions to E_{tot}, namely, the energy in the external field E_{ext} [Fig. 3(b)], exchange energy E_{exch} [Fig. 3(c)], and stray field energy E_{dem} [Fig. 3(d)]; small magnetocrystalline anisotropy of Permalloy was neglected, so that the anisotropy energy $E_{an}=0$. All energies are evaluated for the magnetization configuration *of the total simulation area* (i.e., *not* only for the point-contact area). Plots shown at Figs. 3(b)–3(d) prove that by the transition $W \rightarrow L_1$, all partial energy contributions decrease, although both the oscillation amplitude and the magnetization gradient *within the point-contact* area for the L_1 mode are much larger than for the W mode. However, strong localization of the magnetization oscillations for the L_1 mode compensates for these increases because for the extended mode W, the *whole* simulation area contributes to the total system energy.

The picture for the second transition $L_1 \rightarrow L_2$ is qualitatively different (see Fig. 4) because here *both* modes are localized. During this transition, the exchange energy E_{exch} [Fig. 4(c)] increases—due to the steeper spatial variation of the magnetization within the point-contact area for the mode L_2 compared to L_1. This exchange energy increase is compensated, first, by the decrease of the stray field (demagnetizing) energy E_{dem} due the formation of a magnetic charge "quadrupole" by the two vortex-antivortex pairs characterising the L_2 type. The stray field energy of such a quadrupole is significantly lower than E_{dem} of the approximately homogeneous magnetization configuration of the L_1-mode core. Second, the average mode energy in the external field E_{ext} also decreases, due to a much smaller magnitude of the average magnetization $\langle m_{av} \rangle$ of the mode core for the L_2 type. Again, the reason for this smaller magnitude of $\langle m_{av} \rangle$ is the more complicated inhomogeneous structure of the L_2 core.

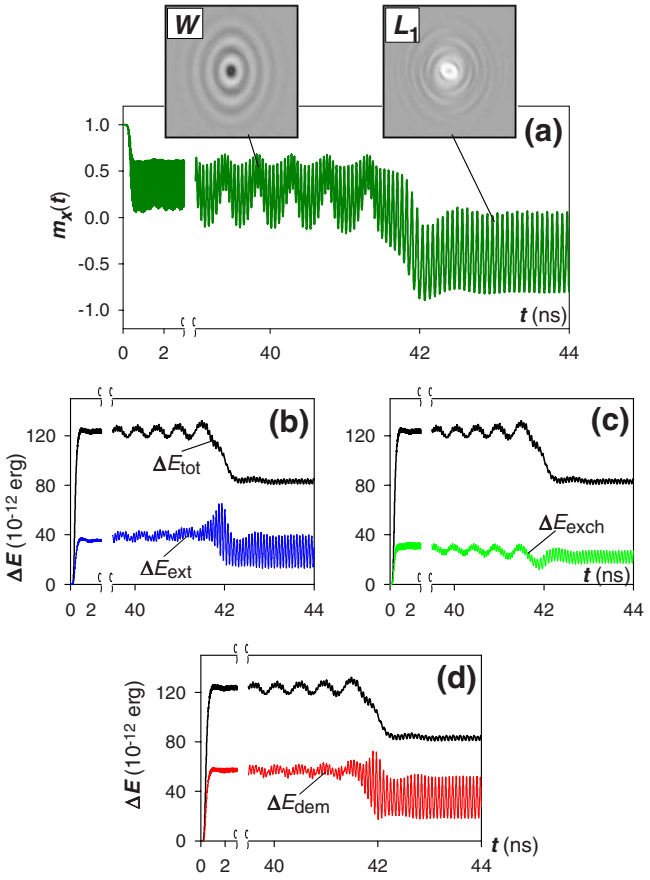

FIG. 3. (Color online) Energy changes of the magnetization configuration of the total simulation area by the transition [see panel (a)] from the extended wave mode W to the first localized mode L_1: (b) change of the energy due to the external field, (c) exchange energy, and (d) demagnetizing energy. Although both the oscillation amplitude and the magnetization gradient within the point-contact area for the L_1 mode are much larger than for W mode, all partial contributions to the total magnetic free energy for the L_1 mode decrease by the transition $W \rightarrow L_1$ because magnetization oscillations in the L_1 mode are strongly localized.

The analysis of the spatial distribution of the oscillation power within the mode cores and the power emission of the localized modes is presented in Fig. 5. The power spectrum shown in these figures is computed by averaging the magnetization oscillation spectra obtained for each discretization cell over all cells (see Ref. 17 for details). The oscillation power maps displayed as insets for each spectral peak present the spatial in-plane distribution of the oscillation power for the $m_y(\mathbf{r})$ component at corresponding frequencies.

In accordance with the snapshots shown in Fig. 1, the spatial power distribution of the magnetization oscillations in the L_1 core shown in Fig. 5(a) has the elliptical symmetry with respect to the point-contact center. The power dependence $P(r)$ on the distance from this center is nonmonotonic; we shall return to this observation later (see discussion be-

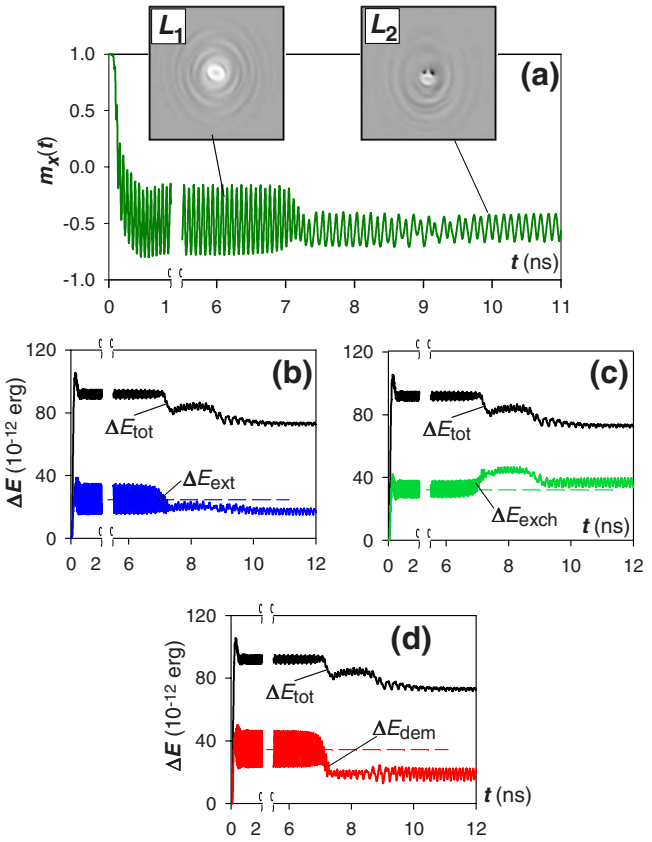

FIG. 4. (Color online) The same as in Fig. 3 for the transition $L_1 \rightarrow L_2$. Here, both modes are localized, so that the external field and the demagnetizing energies decrease due to a more inhomogeneous magnetization configuration of the L_2 mode in the mode localization area (resulting in the decrease of the total energy), whereby the exchange energy increases for the same reason.

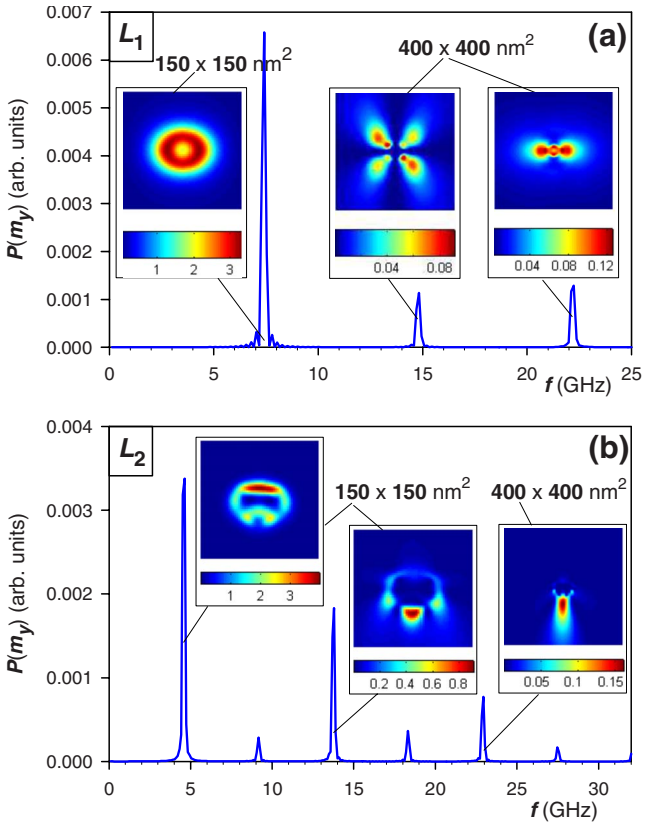

FIG. 5. (Color online) Oscillation power spectra of the perpendicular magnetization component (m_y) averaged over the whole simulation area for localized modes (a) L_1 and (b) L_2. Spatial maps of the oscillation power for corresponding peaks give mode profiles (left maps) and power emission patterns out of the point-contact area. Note that spatial power maps correspond to different physical sizes as written on the figure to ensure the representation of oscillations with different localization degrees with an adequate resolution.

low). Spatial maps for spectral peaks with the frequency higher than the homogeneous FMR frequency f_{FMR} give the pattern of the energy emission out of the point-contact area for this mode (because magnetization oscillations with frequencies $f > f_{\mathrm{FMR}}$ can propagate in a thin film as "normal" spin waves). One can see that the angular distribution of this energy emission is highly anisotropic, whereby for different frequencies the energy is emitted in different directions. This radiation anisotropy should be explicitly taken into account in experiments and technical applications where the synchronization of the nanocontact oscillators in the in-plane geometry is aimed. In addition, our results demonstrate that numerical simulations where the spin-torque effect in nanocontacts is simulated via an artificial "localized magnetic field" (like those presented in Ref. 18), lead to a qualitatively incorrect picture of the power emission out of the point-contact area. Hence, such oversimplified simulations can by no means be used for the analysis of spin-current-induced magnetization excitations in such systems, not to mention the optimization of the nanocontact oscillator synchronization.

The spatial structure of the oscillation power distribution for the L_2 mode [see Fig. 5(b)] is highly complicated already for the mode core [leftmost inset in Fig. 5(b)]. The energy emission pattern is also more complicated than for the L_1 mode [see middle and right insets in Fig. 5(b)]; in addition, the preferred direction of the energy emission changes with the current strength a_J (results not shown). We also note that the average oscillation power at the basic frequency of this mode is much lower than the corresponding power for the L_1 mode [see Fig. 1(b)], which is also due to a more inhomogeneous magnetization configuration within the mode core (region under the point-contact area).

We begin the discussion of our results with their comparison to known analytical theories.

The extended wave mode. The propagating wave mode W, which in our simulations is excited first when the current is increased, corresponds to the linear mode studied by Slonczewski.[8] The threshold current I_{th} for the excitation of this mode can be written for our purposes in the form proposed in Ref. 11 as

$$I_{\mathrm{th}} \approx \frac{1}{\sigma}\left[1.86\frac{D(H_0)}{R_c^2} + \Gamma(H_0)\right], \qquad (1)$$

where the common factor σ depends on the magnetic layer thickness d, point-contact area $S_c = \pi R_c^2$, material saturation

magnetization M_S, and the spin polarization degree P of the current as $\sigma = g\mu_B P/(2|e|M_S dS_c)$. The first term on the right-hand side of Eq. (1) describes the energy loss due to the energy flow carried out of the point-contact area by the extended circular (elliptical) wave. This term is proportional to the spin-wave dispersion $D(H_0)$, which for the field-in-plane geometry has the form

$$D(H_0) = \frac{2\gamma A}{M_S}\frac{H_0 + 2\pi M_S}{\sqrt{H_0(H_0 + 4\pi M_S)}}. \quad (2)$$

The normal energy dissipation within the point-contact area is given by the second term on the right-hand side of Eq. (1), which for the same geometry is $\Gamma(H_0) = \gamma\lambda(H_0 + 2\pi M_S)$. Taking into account that the product of the coefficient σ and the current strength I is related to our spin-torque magnitude $a_J = \hbar IP/(2|e|M_S^2 dS_c)$ (Ref. 19) via $\sigma I = \gamma M_S a_J$, it is easy to derive the analytical threshold value $a_{J,\mathrm{th}}^{\mathrm{an}}$ for the onset of the Slonczewski mode,

$$a_{J,\mathrm{th}}^{\mathrm{an}} = \frac{H_0 + 2\pi M_S}{M_S}\left[\frac{1.86}{R_c^2}\frac{2A}{M_S}\frac{1}{\sqrt{H_0(H_0 + 4\pi M_S)}} + \lambda\right]. \quad (3)$$

Substituting all the values which have been used in our simulations ($H_0 = 1000$ Oe, $M_S = 640$ G, $R_c = 20$ nm, $A = 1.0 \times 10^{-6}$ erg/cm, $\lambda = 0.02$), we obtain $a_{J,\mathrm{th}}^{\mathrm{an}} \approx 3.94$. The good agreement of this value with the threshold obtained in simulations $a_{J,\mathrm{th}}^{\mathrm{num}} \approx 3.55(\pm 0.02)$ can be viewed as an evidence for the good quality of either the simulation software or approximations used by the derivation of Eq. (1); the latter involve mainly the neglect of the group velocity anisotropy in the field-in-plane geometry.

Localized mode L_1. This first type of the localized mode which existence was demonstrated by us for the first time in Ref. 12 and 16 corresponds most probably to the localized nonlinear "bullet," which was predicted and thoroughly analyzed using the nonlinear dynamics methods by Slavin and Tiberkevich.[11] First of all, we point out that the frequencies of our mode [$f(L_1) \approx 7.25-7.45$ GHz] are very close to those predicted in Ref. 11 for the same set of magnetic parameters ($f_{\mathrm{bull}} \approx 7.4-7.8$ GHz). A very important feature also is that these frequencies are definitely below the homogeneous FMR frequency $f_{\mathrm{FMR}} \approx 8.42$ GHz for the studied thin film.

Second, our mode L_1 is also localized, as it is the bullet mode of Slavin and Tiberkevich. Comparison of the power dependencies on the distance to the contact center $P(r)$ for the propagating wave mode W and the L_1 mode is shown in Fig. 6. It can be seen that although the normalized oscillation power of the L_1 mode near the point-contact center is larger than that of the W mode, for $r \gg R_c$, the oscillation power decays for the L_1 mode much faster than for the W mode. From the left inset to Fig. 6, it can be seen that the W-mode power decays as $1/r$. [We note in passing that due to the Gilbert dissipation, the decay law of the W mode $P(r) \sim (1/r)\exp(-r/r_{\mathrm{dec}}^{(W)})$ contains in principle also an exponential factor; however, analytical estimates give for the corresponding decay radius the value $r_{\mathrm{dec}}^{(W)} \sim T_{\mathrm{osc}} v_{\mathrm{gr}}/\lambda \sim 10^4$ nm, so that this exponent cannot be seen for the simulated area size used here.] In contrast to the W mode, the localized bullet mode

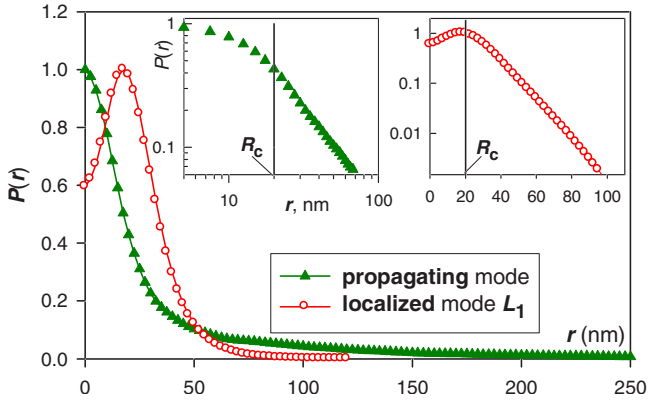

FIG. 6. (Color online) Mode profiles [as the normalized magnetization oscillation power $P(r)$, r being the distance to the contact center] for the propagating wave mode W (triangles) and the first localized mode L_1. Note the nonmonotonic profile of the localized mode. The left inset shows that for $r \gg R_c$(=20 nm), the W mode decays as $1/r$ (note the double-logarithmic coordinates), and the right inset shows that the L_1 mode decays exponentially (note the logarithmic ordinate scale) with the decay radius $r_{\mathrm{dec}}^{(L1)} \approx 12$ (±1) nm of the same order of magnitude as R_c (see text for details).

should decay exponentially with the decay radius $r_{\mathrm{dec}}^{(L_1)} \sim R_c$.[11] Indeed, the exponential fit for the $P(r)$ dependence of the L_1 mode (right inset in Fig. 6) results in the value $r_{\mathrm{dec}}^{(L_1)} = 12(\pm 1)$ nm (in our geometry $R_c = 20$ nm).

However, there exist also important discrepancies between our simulation results and analytical predictions of Slavin and Tiberkevich. First of all, in simulations, the localized mode discussed above is excited *after* the propagating wave mode, whereas according to the analytical theory, the excitation threshold of the bullet mode should be much smaller than for the linear (Slonczewski) mode. We attribute this difference to the circumstance that, first, we start from the homogeneous magnetization state increasing the current value and, second, we do not include thermal fluctuations. Hence, the mode which is topologically the closest one to the homogeneous state, i.e., the linear mode, is excited first. Thus, we suppose that if we would be able to perform simulations during a sufficiently long time including thermal fluctuations, the localized mode would be excited for a_J values below the threshold for the W mode. Unfortunately, such simulations are out of the time range for the state-of-the-art micromagnetic codes, in particular, because thermal fluctuations reduce the accuracy of the numerical integration method by at least 1 order of magnitude (thus requiring the corresponding decrease of the time step for the prescribed accuracy). This effect is especially strong in systems with small discretization cells, as it is the case for the problem under study.

A strong support for the latter argument follows from the fact that the average system energy is strongly *decreased* by the dynamical transition $W \rightarrow L_1$ (see Fig. 3 and the discussion above). Hence, we argue that in the presence of thermal fluctuations which allow to surmount the energy barrier required to excite the localized mode, this mode should be excited first (see discussion in Ref. 11 about the finite mode amplitude of the bullet at its excitation threshold).

Another important difference between our simulations and analytical results of Slavin and Tiberkevich is the *nonmonotonic* mode profile of the L_1 mode immediately after this mode appears (see Fig. 6), whereby analytical calculations predict the *monotonic* power decay of the bullet mode with increasing distance to the contact center. Again, this discrepancy can be easily understood assuming that the localized mode observed in our simulations corresponds to the bullet mode far above its excitation threshold. Thus, analytical prediction for the mode profile given in Ref. 11 for current near the excitation threshold would be invalid for such large currents, where a more complicated mode profile should exist. We also point out that the nonmonotonic mode profile observed in our simulations is the necessary precursor for the transition to the second type of the localized mode L_2 with a highly complicated core magnetization configuration.

Comparison to the experimental data. Before we proceed with the comparison of our data with experimental results, we would like to establish a relation between the current strength used in a real experiment and the value of the spin-torque magnitude a_J employed in our simulations. As mentioned above, in the simplest theoretical approximation, the corresponding relation in Gaussian units is $a_J = \hbar IP/(2|e|M_S^2 dS_c)$, where the only unknown parameter is the current polarization degree P. By adopting, e.g., the value $P=0.3$ (see corresponding estimations in Ref. 6) and taking into account the relation between current units in Gaussian system and SI, we obtain that for the geometry using here $a_J=1$ corresponds to $I \approx 2.6$ mA.

We remind the reader that by simulating the magnetization dynamics, we have made here several approximations: neglected the interaction with the fixed magnetic layer, the influence of the Oersted field, and thermal fluctuations. Nevertheless, comparing our data with the results of Rippard *et al.*,[9] we can explain some important experimental findings. First of all, it is clear that Rippard *et al.* observed the localized mode of the first type (L_1 mode), as it was also suggested in Ref. 11. This conclusion is based, first, on the perfect agreement of frequencies between our L_1 mode with $f(L_1) \approx 7.3$ GHz and the mode observed in Ref. 9 (for $H_0 = 1000$ Oe, this frequency for the maximal microwave power was $f_{\text{expt}} \approx 7.2$ GHz, see Fig. 1 in Ref. 9); it is important to note that our simulations do not contain any adjustable parameters. Additional strong indication for the L_1 mode is that the frequency of our simulated L_1 mode decays *linearly* with increasing the spin-torque magnitude a_J over the wide range of a_J values, in a qualitative agreement with the linear decrease of the oscillation frequency measured experimentally (see inset to Fig. 1(b) in Ref. 9). We point out that the frequency of the propagating wave mode decays with the current strength *nonlinearly*, as it can be clearly seen from our Fig. 1(a).

Another important experimental fact that we can explain in our simulations is the abrupt disappearance of the microwave signal observed in Ref. 9 when the current was increased beyond ~8.5 mA. Namely, according to our results, at the second critical current value $a_{\text{cr}}^{(2)}$, the L_1 mode decays to the second type of the localized mode L_2. For this L_2 mode, the oscillation power predicted by our simulations is more than five times smaller than for the L_1 mode. Oscillations with such a small power, additionally masked by thermal noise, could probably not be detected in a real experiment.

The most important disagreement with simulations remains the absence of the propagating W mode in the real experiment.[9] The reason why such a mode was not observed could be the same as discussed above when we compared our results with analytical predictions concerning the bullet mode.[11] Namely, if the excitation threshold for the localized mode is lower than that for the propagating wave mode, this mode could be experimentally excited first due to thermal fluctuations, which could assist in overcoming the energy barrier required to excite the localized mode. If this is correct, it might be possible to observe the propagating wave mode in the field-in-plane setup by performing experiments at low temperature and taking special precautions against the Joule heating of the nanocontact area.

B. Effects of a nonlinear damping

Taking into account that the constant damping coefficient λ for the standard Gilbert damping considered above leads to the unphysical decrease of the dissipated power with the growing amplitude of magnetization oscillations, Tiberkevich and Slavin[14] proposed to introduce a phenomenological dependence of this damping coefficient on the magnetization change rate $d\mathbf{M}/dt$. As shown in Ref. 14, the first nontrivial term in such a dependence should have the form $\lambda = \lambda_G(1+q_1\xi)$, where the quantity $\xi = (d\mathbf{m}/dt)^2/(4\pi\gamma M_S)^2$ includes the dependence of damping on the magnetization change rate ($\mathbf{m}=\mathbf{M}/M_S$). The value of the nonlinear coefficient q_1 should be calculated from the microscopic theory, so in the present study, we consider it as a phenomenological quantity and explore the dependence of the system properties on the value of q_1.

Results of our simulations of magnetization oscillations driven by a spin-polarized current in the same point-contact setup as described above for various nonlinear coefficients q_1 are shown in Fig. 7 (weak nonlinearity $q_1=1$) and Fig. 8 (strong nonlinearity $q_1=10$ and $q_1=20$) in comparison with the linear damping case discussed in the previous section.

The influence of a small nonlinearity ($q_1=1$) on the magnetization dynamics in the extended wave mode W is weak: nonlinear damping slightly reduces the oscillation power and amplitude [see Fig. 7(b)], thus increasing—also slightly—the oscillation frequency when compared to the linear case [Fig. 7(a)]. The a_J threshold where the W mode loses its stability also gets slightly larger. However, the existence region of the localized modes changes in a qualitative way: immediately above the first critical value $a_{\text{cr}}^{(1)}$, the system exhibits a transition to a *second* type of the localized mode L_2, and *not* to L_1, as was the case for the linear damping. For still larger currents, the system oscillation mode changes to L_1, and by further increase of a_J, the transition back to L_2 takes place, so that the current region $a_J(L_1)$ where the localized mode of the first kind L_1 exists is limited both from below and from above by the regions where the second localized L_2 mode determines the magnetization dynamics: $a_J^{\min}(L_1) < a_J(L_1) < a_J^{\max}(L_1)$. When the value of the nonlinear coefficient q_1

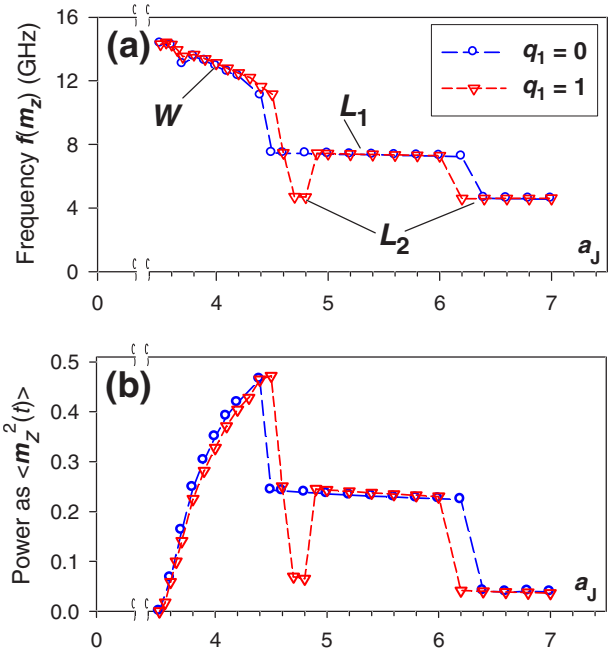

FIG. 7. (Color online) Dependencies of the (a) frequency and (b) oscillation power on the spin-torque magnitude a_J for the small nonlinear damping $q_1=1.0$ (triangles) compared with the linear damping case (circles). It can be seen that for the nonlinear damping, the a_J region where the mode L_1 exists is surrounded both from below and above by the existence regions of the L_2 mode.

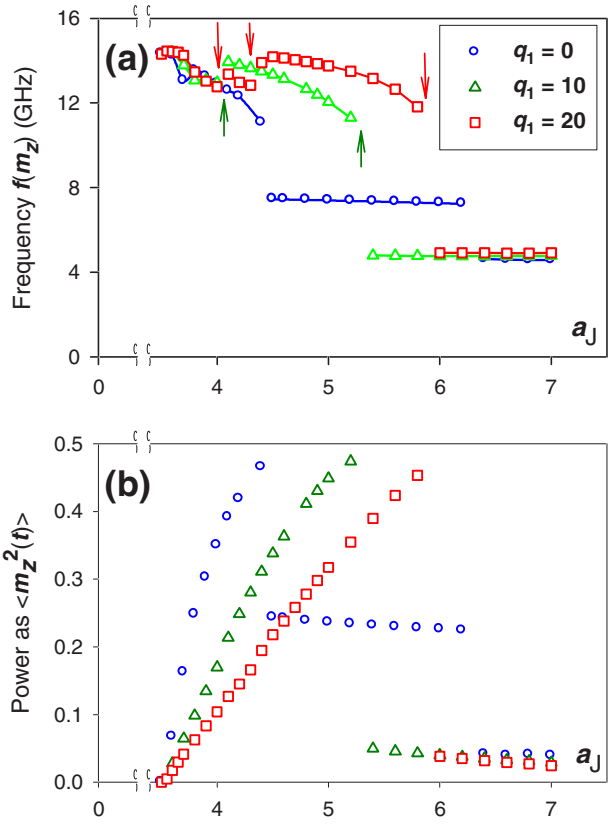

FIG. 8. (Color online) The same as in Fig. 7 for the large nonlinear damping $q_1=10.0$ (triangles) and $q_1=20.0$ (squares) compared also to the linear damping case (circles). For such large values of the nonlinear parameter q_1, the first type of the localized mode L_1 does not exist anymore. Note also several frequency jumps within the existence region of the W mode (shown with arrows).

gets larger, the lower border of this interval $a_J^{\min}(L_1)$ increases, whereby the upper border $a_J^{\max}(L_1)$ decreases, so that for a sufficiently strong nonlinearity q_1, the first type of the localized mode does not exist anymore (see Fig. 8).

For large values of the nonlinear parameter q_1, also another qualitative effect has been observed: frequency jumps occur within one and the same mode type, extended wave mode W, as shown in Fig. 8(a). The number and magnitude of these jumps are determined by the concrete value of q_1: we have found, e.g., one jump within the W mode for $q_1=10$ and 2 such jumps for $q_1=20$. These frequency jumps do not lead to any qualitative changes of the magnetization oscillation pattern but are of course accompanied by corresponding (relatively small) jumps in the spin-wave vector magnitude and by small kinks on the power dependence $P(a_J)$ [Fig. 8(b)].

The relatively narrow stability region of the first localized mode (which additionally narrows by increasing the nonlinear parameter q_1) results in a natural question whether this mode is stable (at least for $T=0$) or it is only dynamically metastable, having the lifetime larger than the numerical simulation reach. Namely, every point on $f(a_J)$ dependencies in Figs. 1, 7, and 8 is the result of a simulation run which corresponds to the physical time $t_{\max}=25$ ns, so that if the L_1 mode is unstable for all a_J values, but for $a_J<a_{\rm cr}^{(2)}$ its lifetime is $\tau_{L_1}>t_{\max}$, then this instability would not be discovered in our simulations. To clarify this question, we have plotted the lifetimes of the L_1 mode as the function of a_J for $a_J>a_{\rm cr}^{(2)}$, i.e., where the L_1 mode decays to L_2 within the accessible simulation time. The obtained dependence $\tau_{L_1}(a_J)$ is shown in Fig. 9 together with the fit $\tau_{L_1}(a_J)=A/|a_J-a_0|^\beta$, which assumes that the lifetime as the function of a_J *diverges* when a_J approaches some critical value a_0. It can be seen that this functional form fits the obtained $\tau_{L_1}(a_J)$ very well. We consider this observation as an indirect evidence that the stabil-

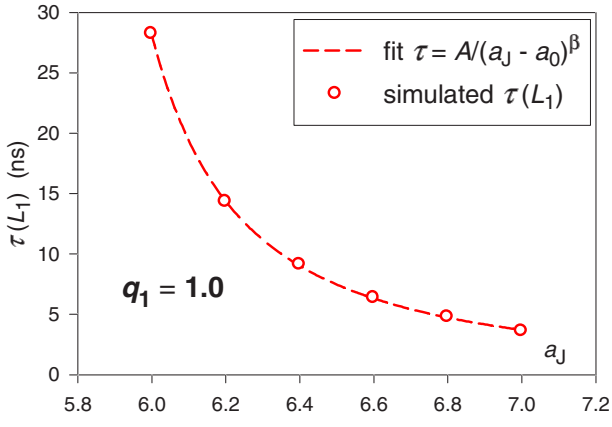

FIG. 9. (Color online) Lifetimes of the first localized mode L_1 for a_J values where this mode decays to the L_2 mode. The fit of the functional form shown in the figure (with $a_0\approx5.6$ and $\beta\approx1.5$) strongly indicates that these lifetimes tend to infinity when a_J decreases, so that the region where the L_1 mode is stable really exists.

ity region for the first localized mode really exists, although the limited number of data for $\tau_{L_1}(a_J)$ in the immediate vicinity of a_0 does not allow to draw the final inference. Concluding this discussion, we would like to mention that, according to our preliminary studies[13] carried out on a double-layer system, the first localized mode may lose its stability also due to the magnetodipolar interaction with the fixed magnetic layer in the point-contact geometry.

IV. CONCLUSION

In this paper, we have studied systematically (using micromagnetic simulations) magnetization excitations driven by the spin-polarized current injected into a thin film via a point contact. We could show that for an external field in the film plane, such excitations may exist in the form of qualitatively different modes. The possible mode types include a *propagating* wave mode *W* as suggested by Slonczewski[8] and two strongly *localized* modes. The core of the first type of these localized modes (L_1) has an approximately homogeneous magnetization state, whereby the magnetization configuration of the second-type mode core (L_2) is strongly inhomogeneous. The localized mode L_1 corresponds most probably to the spin-wave bullet investigated analytically by Slavin and Tiberkevich.[11] Comparison with the experimental results of Rippard *et al.*[9] leads to the conclusion that the microwave resistance oscillations observed in Ref. 9 are caused by the localized mode of type L_1, whereas the disappearance of oscillations by increasing current corresponds to the transition $L_1 \rightarrow L_2$. Further, we have shown that the power emission by both types of the localized modes is strongly anisotropic, which is very important for potential applications of the point-contact devices including the synchronization of various point-contact oscillators.

We have also demonstrated that a weak nonlinearity of the damping included into the LLG equation of motion shifts the current threshold values corresponding to the transition between different mode types. Strong nonlinearity causes frequency jumps already within a propagating wave mode and leads to a complete disappearance of the first localized mode L_1.

ACKNOWLEDGMENTS

We greatly acknowledge many useful discussions with A. Slavin. Financial support of the Deutsche Forschungsgemeinschaft (Research Grant No. BE 2464/4-1 in frames of the Priority Program SPP 1133 "Ultrafast magnetization dynamics") is also acknowledged.

[1] J. C. Slonczewski, J. Magn. Magn. Mater. **159**, L1 (1996).
[2] L. Berger, Phys. Rev. B **54**, 9353 (1996).
[3] J. Z. Sun, J. Magn. Magn. Mater. **202**, 157 (1999); M. Tsoi, A. G. M. Jansen, J. Bass, W.-C. Chiang, M. Seck, V. Tsoi, and P. Wyder, Phys. Rev. Lett., **80**, 4281 (1998).
[4] Y. Tserkovnyak, A. Brataas, G. E. W. Bauer, and B. I. Halperin, Rev. Mod. Phys. **77**, 1375 (2005); M. D. Stiles and J. Miltat, in *Spin Dynamics in Confined Magnetic Structures III*, Springer Series Topics in Applied Physics Vol. 101 (Springer-Verlag, Berlin, 2006).
[5] S. I. Kiselev, J. C. Sankey, I. N. Krivorotov, N. C. Emley, R. J. Schoelkopf, R. A. Buhrman, and D. C. Ralph, Nature (London) **425**, 380 (2003); S. I. Kiselev, J. C. Sankey, I. N. Krivorotov, N. C. Emley, A. G. F. Garcia, R. A. Buhrman, and D. C. Ralph, Phys. Rev. B **72**, 064430 (2005); I. N. Krivorotov, N. C. Emley, J. C. Sankey, S. I. Kiselev, D. C. Ralph, and R. A. Buhrman, Science **307**, 228 (2005); Q. Mistral, J.-V. Kim, T. Devolder, P. Crozat, C. Chappert, J. A. Katine, M. J. Carey, and K. Ito, Appl. Phys. Lett. **88**, 192507 (2006); Y. Acremann, J. P. Strachan, V. Chembrolu, S. D. Andrews, T. Tyliszczak, J. A. Katine, M. J. Carey, B. M. Clemens, H. C. Siegmann, and J. Stöhr, Phys. Rev. Lett. **96**, 217202 (2006); J. C. Sankey, P. M. Braganca, A. G. F. Garcia, I. N. Krivorotov, R. A. Buhrman, and D. C. Ralph, Phys. Rev. Lett. **96**, 227601 (2006).
[6] X. Waintal, E. B. Myers, P. W. Brouwer, and D. C. Ralph, Phys. Rev. B **62**, 12317 (2000); M. D. Stiles and A. Zangwill, *ibid.* **66**, 014407 (2002); J. C. Slonczewski, J. Magn. Magn. Mater. **247**, 324 (2002); J. Xiao, A. Zangwill, and M. D. Stiles, Phys. Rev. B **70**, 172405 (2004); L. Berger, *ibid.* **72**, 100402(R) (2005); J.-V. Kim, *ibid.* **73**, 174412 (2006).
[7] J. Z. Sun, Phys. Rev. B **62**, 570 (2000); J. Miltat, G. Albuquerque, A. Thiaville, and C. Vouille, J. Appl. Phys. **89**, 6982 (2001); Z. Li and S. Zhang, Phys. Rev. B **68**, 024404 (2003); X. Zhu, J.-G. Zhu, and R. M. White, J. Appl. Phys. **95**, 6630 (2004); J.-G. Zhu and X. Zhu, IEEE Trans. Magn. **40**, 182 (2004); K. J. Lee, A. Deac, O. Redon, J. P. Nozieres, and B. Dieny, Nat. Mater. **3**, 877 (2004); B. Montigny and J. Miltat, J. Appl. Phys. **97**, 10C708 (2005); J. Xiao, A. Zangwill, and M. D. Stiles, Phys. Rev. B **72**, 014446 (2005).
[8] J. C. Slonczewski, J. Magn. Magn. Mater. **195**, 261 (1999).
[9] W. H. Rippard, M. R. Pufall, S. Kaka, S. E. Russek, and T. J. Silva, Phys. Rev. Lett. **92**, 027201 (2004).
[10] A. N. Slavin and P. Kabos, IEEE Trans. Magn. **MAG-41**, 1264 (2005).
[11] A. Slavin and V. Tiberkevich, Phys. Rev. Lett. **95**, 237201 (2005).
[12] D. V. Berkov, J. Magn. Magn. Mater. **300**, 159 (2006).
[13] D. V. Berkov and N. L. Gorn, J. Appl. Phys. **99**, 08Q701 (2006).
[14] V. Tiberkevich and A. Slavin, Phys. Rev. B **75**, 014440 (2007).
[15] D. V. Berkov and N. L. Gorn, MICROMAGUS, package for micromagnetic simulations (http://www.micromagus.de).
[16] D. V. Berkov and N. L. Gorn, The Joint European Magnetic Symposium, Dresden, Germany, September 2004 (unpublished); D. V. Berkov and N. L. Gorn, Moscow International Symposium on Magnetism, June 2005, Moscow, Russia (unpublished).
[17] D. V. Berkov and N. L. Gorn, Phys. Rev. B **72**, 094401 (2005).
[18] S. Choi, S.-K. Kim, V. E. Demidov, and S. O. Demokritov, Appl. Phys. Lett. **90**, 083114 (2007).
[19] I. N. Krivorotov, D. V. Berkov, N. L. Gorn, N. C. Emley, J. C. Sankey, D. C. Ralph, and R. A. Buhrman, Phys. Rev. B **76**, 024418 (2007).
[20] S. M. Rezende, F. M. de Aguiar, and A. Azevedo, Phys. Rev. B **73**, 094402 (2006).